Acta Polytechnica **62**(4):418–426, 2022
https://doi.org/10.14311/AP.2022.62.0418

Published by the Czech Technical University in Prague

DISINFECTION PERFORMANCE OF AN ULTRAVIOLET LAMP: A CFD INVESTIGATION

Cuong Mai Bui, Nguyen Duy Minh Phan*, Ngo Quoc Huy Tran, Le Anh Doan, Quang Truong Vo, Duy Chung Tran, Thi Thanh Vi Nguyen, Duc Long Nguyen, Van Sanh Huynh, Tran Anh Ngoc Ho

The University of Danang - University of Technology and Education, 48 Cao Thang, Danang 550000, Viet Nam

* corresponding author: pndminh@ute.udn.vn

Abstract.

Ultraviolet(UV)-based devices have shown their effectiveness on various germicidal purposes. To serve their design optimisation, the disinfection effectiveness of a vertically cylindrical UV lamp, whose wattage ranges from $P = 30$–$100\,\mathrm{W}$, is numerically investigated in this work. The UV radiation is solved by the Finite Volume Method together with the Discrete Ordinates model. Various results for the UV intensity and its bactericidal effects against several popular virus types, i.e., *Corona-SARS*, *Herpes* (type 2), and *HIV*, are reported and analysed in detail. Results show that the UV irradiance is greatly dependent on the lamp power. Additionally, it is indicated that the higher the lamp wattage employed, the larger the bactericidal rate is observed, resulting in the greater effectiveness of the UV disinfection process. Nevertheless, the wattage of $P \leq 100\,\mathrm{W}$ is determined to be insufficient for an effective disinfection performance in a whole room; higher values of power must hence be considered in case intensive sterilization is required. Furthermore, the germicidal effect gets reduced with the viruses less sensitive to UV rays, e.g, the bactericidal rate against the *HIV* virus is only $\sim$8.98 % at the surrounding walls.

Keywords: UV-C, disinfection, discrete ordinates, *Corona-SARS*, CFD.

1. Introduction

The worldwide outbreak of Coronavirus (COVID-19), which terribly affects human health and the world economy, has drawn a great awareness of infectious diseases' danger. Numerous intensive studies have been carried out to improve the disinfection efficiency in hospitals where many patients with serious underlying medical conditions stay [1–5]. In order to prevent the virus spread, various controlling techniques, such as air filtration, heat sterilization, chemical disinfectants, and Ultraviolet Germicidal Irradiation (UVGI), have been employed [6]. Amongst them, the last one uses the spectral sensitivity to *Deoxyribonucleic Acid* (DNA) of Ultraviolet (UV) light of wavelength ranging between 100–280 nm [7]. In detail, under the so-called UVC conditions, the photochemical changes in nucleic acids would deactivate the reproduction of microorganisms [8]. To mention some advantages of this approach, in addition to dealing with virus growth efficiently within a short time, the UVGI approach could save a large amount of operating and maintenance costs. Furthermore, with the no-touch mechanism, UVGI is supposed to ensure a better safety for human activities and the environment during the disinfection process as compared to chemical treatments [9].

Recently, many UV-C-based devices and autonomous robots are developed for disinfection purposes in hospitals and/or medical centers [10–13]. To optimise their design, factors directly affecting the germ-killing efficiency, e.g., UV dose and intensity, should be taken into account. In recent years, the advanced development of the Computational Fluid Dynamics (CFD) approach allows to better predict the irradiation distribution and physical phenomenon occurring during the UV germicidal process. In fact, numerical simulation was first employed to investigate the water treatment performance of UV reactors. Pan and Orava [14] indicated that CFD integrated with fluence modelling approach could be an important tool to determine flow and radiation field characteristics. Ho [15] numerically investigated the influences of wall reflection and refraction at separating material interfaces (e.g., quartz sleeve or lamp surface) on the water disinfection inside a chamber; the Discrete Ordinates (DO) method was adopted to solve the radiation transfer equation. As illustrated, simulation results for the radiation intensity could be overestimated around the lamp but underestimated further away from it once the reflection and refraction were not considered at the quart sleeve. Additionally, Sobhani and Shokouhmand [16] investigated the influences of the lamp power, the flow rate, and the water temperature using both experimental and numerical approaches. It was claimed that the lower the flow rate and/or the greater the lamp power, the higher the UV reactors' efficiency was seen. Recently, the

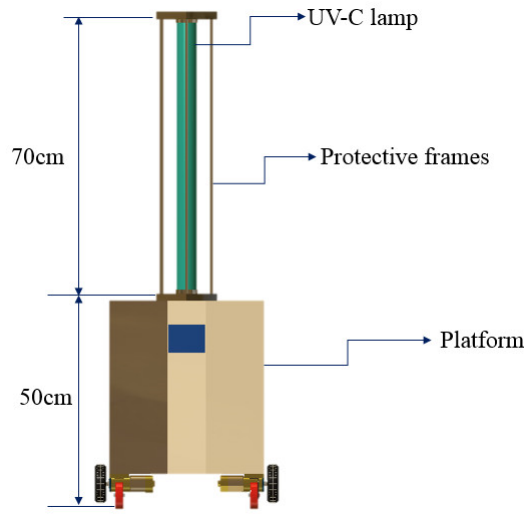

FIGURE 1. Example of a simple UV disinfection device.

CFD approach has been widely utilised to predict air disinfection performance. Capetillo et al. [17] and then Atci et al. [18] studied the UV germicidal efficiency in heating, ventilation, and air conditioning (HVAC) systems. Different arrangements of single and/or multiple lamps were assessed to determine the optimal in-duct configurations. Various results for the airflow field, the UV irradiation distribution, and UV dose were reported and analysed in detail therein. Moreover, a Lagrangian approach was realised for modelling the UV bactericidal influences at Reynolds numbers of $\mathrm{Re} = 4.11 \times 10^4 - 8.22 \times 10^4$ [19]. It was noted that the results obtained were well in line with experimental data; this technique showed a better prediction over an Eulerian one. Results also indicated that the disinfection rate for *P. alcaligenes* and *E. coli* viruses was 100 %. For the *Coronavirus*, Buchan et al. [20] carried out a series of simulations for a populated room with a UV-C device. It was indicated that the far UV-C lighting can increase the bactericidal rate up to 80 % rather than using a conventional ventilation system.

To our best knowledge, the research on the UV disinfection performance in hospitals is still very scarce [21]. In this study, we are aiming at evaluating the coverage region and then the bactericidal effects of a vertical UV lamp using a numerical approach. It is noted that this setting is equivalent to the simplest design of a disinfection device (see Figure 1). As a preliminary study, the influences of airflow and temperature variation are considered to be neglected.

The rest of this paper is organized as follows: theory background including governing equations and numerical approach is provided in Section 2; Section 3 presents and analyses the simulation results; some concluding remarks and recommendations for future works are revealed in Section 4.

2. Theory Background

2.1. Modelling of UV Irradiance

The UV irradiance is governed by the radiative transfer equation (RTE) as follows:

$$\frac{dI(\mathbf{r},\mathbf{s})}{ds} + (\alpha+\sigma_s)I(\mathbf{r},\mathbf{s}) = \alpha n^2 \frac{\sigma T^4}{\pi} + \frac{\sigma_s}{4\pi}\int_0^{4\pi} I(\mathbf{r},\mathbf{s}')\Phi(\mathbf{s}\cdot\mathbf{s}')d\Omega' \,. \quad (1)$$

Here, I is the radiation intensity; $\mathbf{r}$, $\mathbf{s}$ and $\mathbf{s}'$ are, in turn, the position, direction, and the scattering direction vectors; respectively, α and σ_s stand for the absorption and scattering coefficients, respectively; n is the refractive index; $\sigma = 5.669 \times 10^{-8}$ W/m^{2}K^4 is the Stefan-Boltzmann constant; T is the local temperature; Φ is the phase function; Ω' is the solid angle.

To numerically solve Equation 1 with a finite discretization of solid angles, the DO radiation model for non-gray radiation is utilised as [15, 22]:

$$\nabla\cdot(I_\lambda(\mathbf{r},\mathbf{s})\mathbf{s}') + (\alpha_\lambda+\sigma_s)I_\lambda(\mathbf{r},\mathbf{s}) = \alpha_\lambda n^2 I_{b\lambda} + \frac{\sigma_s}{4\pi}\int_0^{4\pi} I(\mathbf{r},\mathbf{s}')\Phi(\mathbf{s}\cdot\mathbf{s}')d\Omega' \,, \quad (2)$$

with I_λ being the spectral intensity, $I_{b\lambda}$ the black body intensity, and α_λ the spectral absorption coefficient.

The correlation between the lamp wattage, P, and the initial intensity, I_0, applied on the UV lamp is expressed as [8]:

$$I_0 = \frac{P}{2\pi r l} \,, \quad (3)$$

with r and l being the radius and length of the UV lamp, respectively.

2.2. Bactericidal rate

The disinfection performance is assessed by the bactericidal rate, b, as [23]:

$$b = (1 - s_v) \times 100\,\% = (1 - e^{-kIt}) \times 100\,\% \,. \quad (4)$$

Here, s_v is the survival rate and t is the exposure duration. Moreover, k is the standard rate constant representing the microorganism susceptibility; the larger the k, the higher the virus sensitivity to the UV rays, and the greater disinfection effectivity [8]. In this work, we focus on three different virus types, whose k vary in a relatively wide range, as follows

- The *Corona-SARS* ($k = 0.1106\,\mathrm{m}^2/\mathrm{J}$) which was responsible for the SARS outbreak in 2003,
- The *Herpes* (type 2) ($k = 0.06569\,\mathrm{m}^2/\mathrm{J}$) which causes itching or blisters on human skin , and
- The *HIV* ($k = 0.00822\,\mathrm{m}^2/\mathrm{J}$) which severely damages the immune system of a human body.

More values of k can be referred in [8].

Mesh	Number of elements	I_A [W/m^2]	I_B [W/m^2]	Running Time [h]
M1	714,150	9.21	2.42	3
M2	1,039,332	9.38	2.33	4.2
M3	1,504,393	9.84	2.28	5
M4	2,196,471	9.86	2.28	8.5

Table 1. Results for the UV intensity at points A and B with various mesh resolutions.

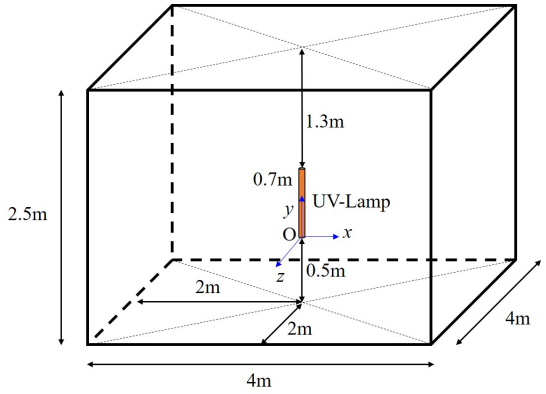

Figure 2. Computational geometry.

Pixelation	I_A [W/m^2]	I_B [W/m^2]
1×1	9.83	2.28
3×3	9.84	2.28
5×5	9.84	2.28

Table 2. Variation in results for intensity at points A and B produced by a 100 W-lamp with different pixel resolutions.

2.3. Simulation Strategy

2.3.1. Computational Geometry and Mesh

A three-dimensional (3D) computational domain mimicking an operating room is built as in Figure 2. The room is 4 m in length, 4 m in width, and 2.5 m in height; the UV lamp is positioned centered and 0.5 m away from the floor. The lamp is of a cylindrical shape; its diameter and length are 0.05 m and 0.7 m, as introduced in [24]. For boundary conditions, we apply a semi-transparent condition for the lamp's surface and an opaque condition for all the surrounding walls. A detailed explanation for these setups can be found in Ho [15].

To handle the calculations, an unstructured tetrahedral mesh with a high resolution near the lamp is generated. Moreover, at least five prisms are created around the lamp's surface to improve the accuracy and stability of the problem (see Figure 3). It is worth noticing that a mesh convergence study has been carried out. A comparison in the boundary of $I = 100\,\mathrm{W/m^2}$ produced by a 100 W-lamp among four mesh resolutions, i.e., M1 (∼714 K elements), M2 (∼1.039 M elements), M3 (∼1.504 M elements), and M4 (∼2.196M elements), is illustrated in Figure 4. It is evident that the deviation becomes negligibly insignificant with the refinement greater than 1.504M elements. In addition, Table 1 reveals the results for the UV intensity at points A and B, which are defined in Figure 5. Mesh M3 is found to be the most optimal since it provides nearly the same values as M4, but is much more computationally efficient. It is, therefore, reasonable to adopt M3 for all simulations. Numerical calculations are conducted with the Finite Volume Method (FVM) in Ansys Fluent v14.5.

2.3.2. Modelling parameters

The parameters characterising angular discretization in the DO model are determined in this part. They include the pixelations (i.e., theta and phi pixels) and the divisions (i.e., theta and phi divisions). The former defines pixel refinements for an overhanging control volume; and the latter controls the angle quantity employed to discrete each octant [22].

Figure 6 compares the irradiation field obtained by different values of pixels. As can be seen, a non-smooth contour on the lamp is found with the pixelations of 1×1; however, the smoothness is improved with a resolution larger than 3×3. Moreover, the irradiation distribution is seen to be identical both qualitatively (see Figure 6) and quantitively (see Table 2) for all the values tested. The pixelation set of 3×3 is, hence, selected.

The effects of the divisions are observed to be considerably more pronounced (see Figure 7). As can be seen, there exists an obvious shift in the irradiation contour when the divisions are varied. The irradiance can be unphysically developed with limited emission directions as the divisions are smaller than 8×8. The larger the number of divisions, the smoother the intensity distribution can be observed. It is noteworthy that the divisions of 3×3 and 10×10 were proposed by Ho [15] and Atci et al. [18], respectively; however, these sets seem to be insufficient to ensure the accuracy in our case. We then adopt the division set of 15×15 as it not only provides an irradiation field very similar to that from the 20×20 one but saves a large computational cost, i.e., 5 hours for the former as compared to 12.5 hours for the latter.

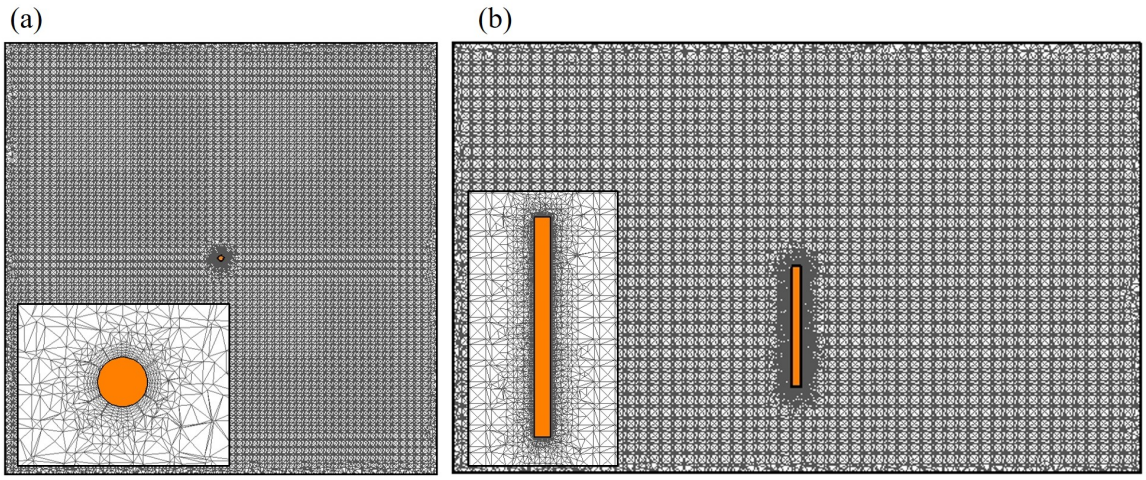

FIGURE 3. Example of mesh employed in (a) the xz-centerplane and (b) the xy-centerplane.

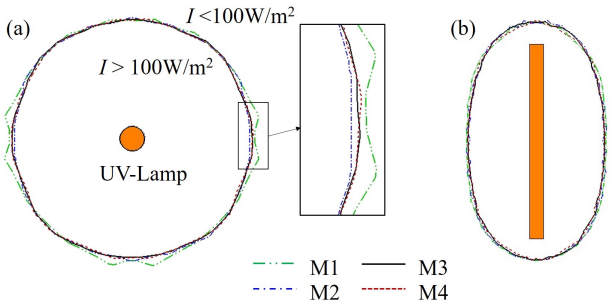

FIGURE 4. Variation in the boundary of $I = 100\,\mathrm{W/m^2}$ produced by a 100 W-lamp in (a) xz-centerplane and (b) the xy-centerplane with various mesh resolutions.

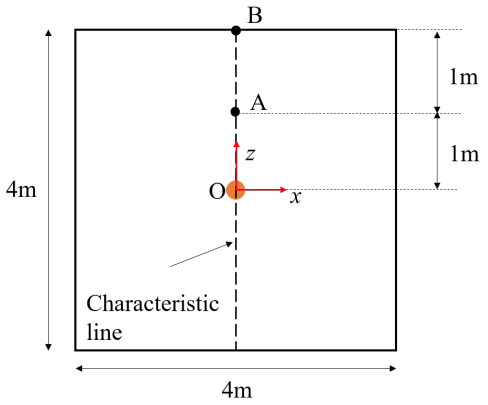

FIGURE 5. Definitions of the characteristic line, point A, and point B.

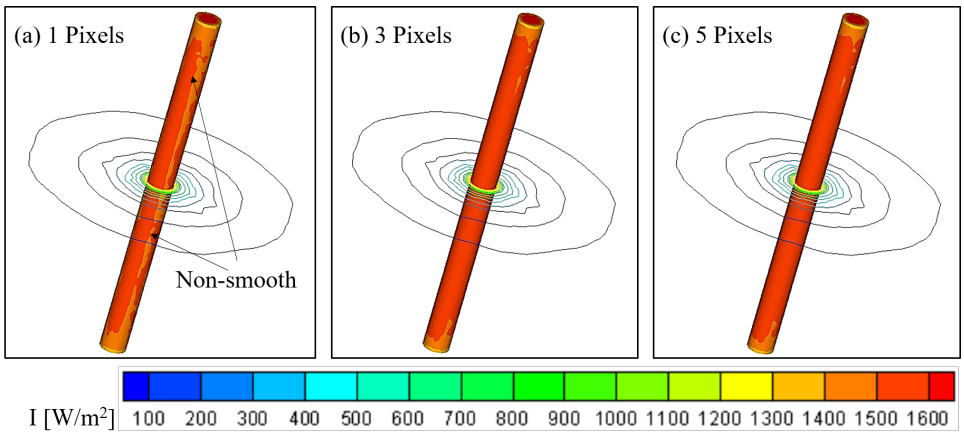

FIGURE 6. Variations in the intensity distribution on the 100 W-lamp and around it in the xz-centerplane with different pixelation sets.

3. Results and Discussion

3.1. UV Irradiance

In this part, the influences of the lamp wattage/power on the UV intensity distribution are presented and discussed. The wattage is varied in the range of $P =$ 30–100 W. The surrounding air absorption is assumed to be neglected in our present work.

Figure 8 shows the UV intensity along the characteristic line produced by various lamp powers. For all cases, the intensity is seen to be extremely high near the lamp's surface but tends to reduce with the

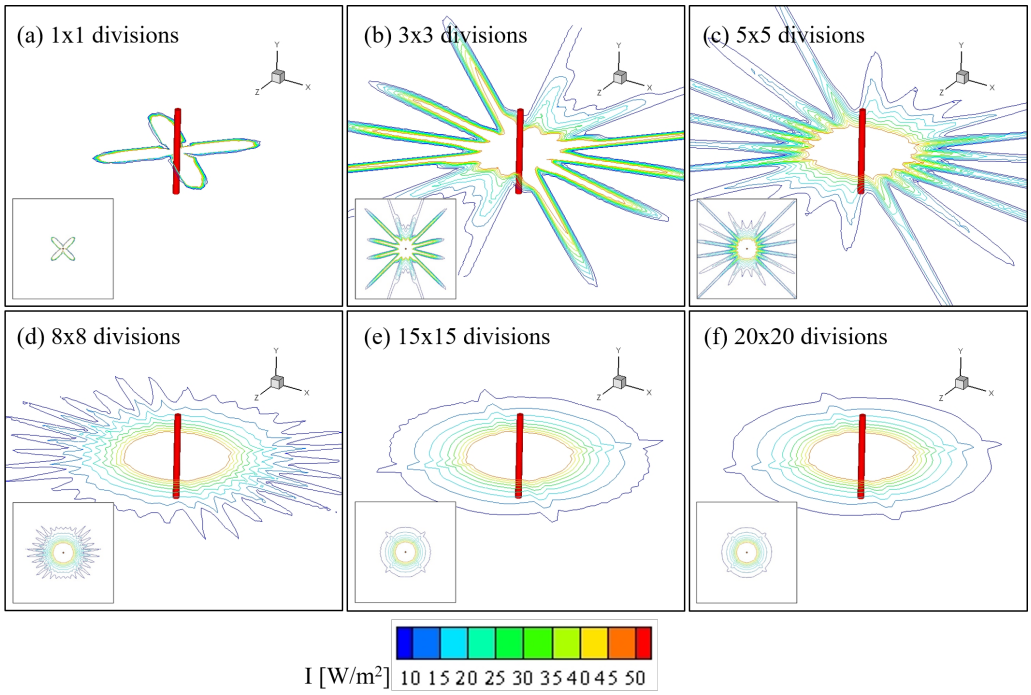

Figure 7. Variations in the irradiation field on the 100 W-lamp and in the xz-centerplane with different division sets.

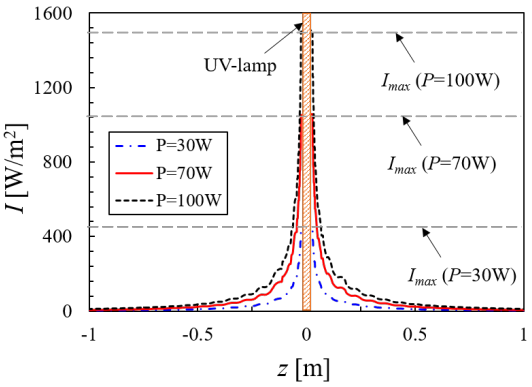

Figure 8. UV intensity distribution along the characteristic line.

increasing distance. The maximum intensity value, I_{max}, is found on the lamp; it is important to note that I_{max} is not always equivalent to the initial intensity I_0. For instance, with a 100 W-lamp, the largest value on the characteristic line is of $I_{max} = 1508.6\,\mathrm{W/m^2}$ being ∼1.65 times greater than that of I_0. This phenomenon is probably due to the radiative emission mechanism and was also observed in [18]. Additionally, the maximum intensity gets drastically smaller as the lower wattage is employed; indeed, I_{max} on the characteristic line reduces by up to ∼3.3 times when P decreases from 100 W to 30 W.

The results for the UV irradiation distribution in the central xz and xy planes are presented in Figure 9. It occurs that the UV intensity variation is significantly more obvious in the horizontal plane. As can be observed, the UV rays are distributed nearly symmetrically in the xy-centerplane. Moreover, the formation of high-intensity regions is noted around the lamp; these zones drastically enlarge with the increasing lamp power. For example, the coverage radius of the UV intensity larger than $50\,\mathrm{W/m^2}$ from a 100 W-lamp is estimated to be 2.6 times greater than that from a 30 W-one; in detail, it is 0.392 m and 0.175 m for the former and the latter, respectively.

3.2. Bactericidal effects

The UV disinfection effectiveness associated with the bactericidal effects of various lamp wattages is reported and analysed in this part. As introduced before, we investigate three different virus types, i.e., the *Corona-SARS*, the *Herpes*, and the *HIV* viruses. The exposure duration is assumed to be fixed at $t = 5\,\mathrm{s}$. In addition, the effective bactericidal rate is chosen to be $b_e = 85\,\%$. Furthermore, the area within which more than 85 % of the total active viruses are eliminated, i.e., $b \geq b_e$, is defined as the effective sterilization zone (see Figure 10).

Figure 11 illustrates the bactericidal effect on the *Corona-SARS* virus. As expected, the higher the lamp wattage employed, the greater the bactericidal effect can be observed in both the central xz and xy planes. As can be observed, the 30 W-lamp generates a relatively small effective sterilization zone; however, this zone is seen to be significantly extended with $P \geq 70\,\mathrm{W}$. Indeed, r_e is increased by ∼1.46 and ∼1.76 times for $P = 70\,\mathrm{W}$ and 100 W, respectively, as compared to that of $P = 30\,\mathrm{W}$ (see Table 3). The effective disinfection is, however, seen to not cover the whole room for all the lamp powers studied in

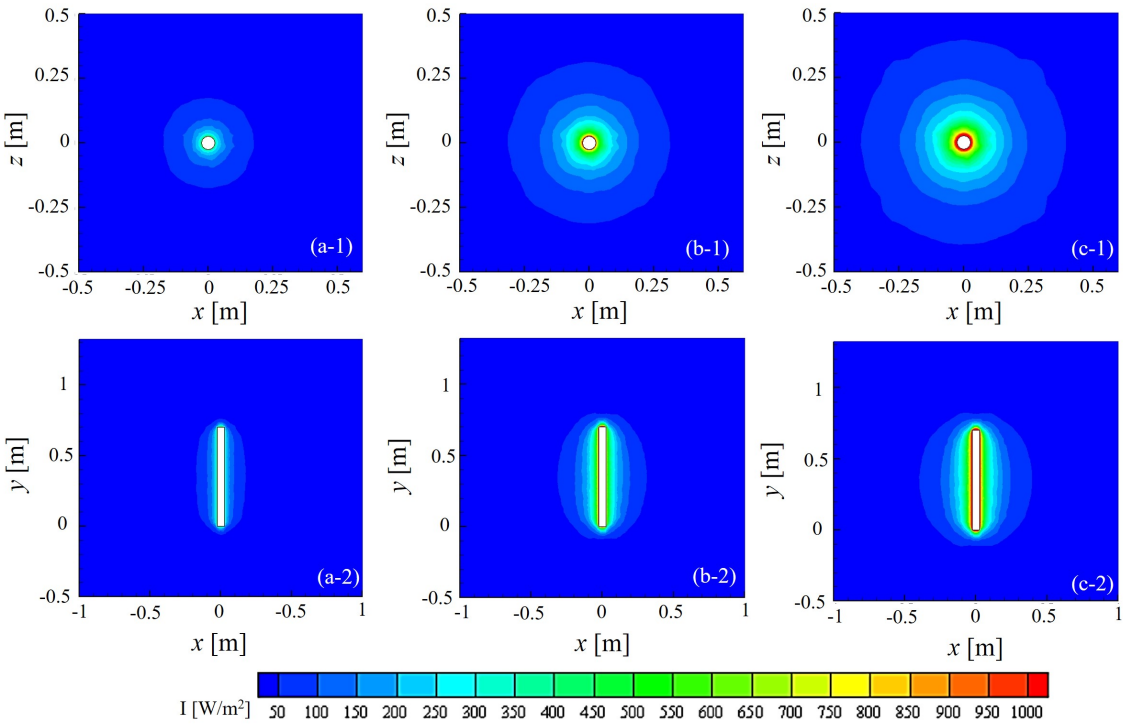

FIGURE 9. Simulated UV irradiation field in (1) the xz-centerplane and (2) the xy-centerplane produced by a UV-lamp of (a) 30 W, (b) 70 W and (c) 100 W.

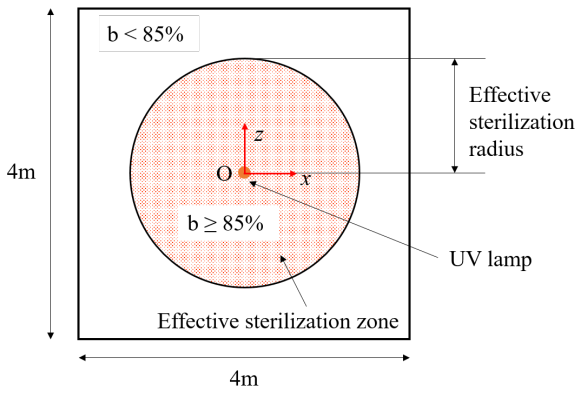

FIGURE 10. Definitions of the effective sterilization zone and its radius, r_e, in the xz-centerplane.

P	*Corona-SARS*	*Herpes*	*HIV*
30 W	0.925 m	0.71 m	0.175 m
70 W	1.365 m	1.075 m	0.325 m
100 W	1.625 m	1.285 m	0.405 m

TABLE 3. Results for r_e of various lamp wattages.

our study. For instance, despite the fact that the bactericidal rate is greatly improved with $P = 100$ W, there still exists a large ineffective sterilization zone above the lamp (see Figure 11c-2), resulting in the high possibility of a large number of viruses still surviving near the ceiling and floor. A higher lamp wattage is, hence, suggested in case absolute disinfection is required.

Figure 12 shows the UV bactericidal performance of a 70 W-lamp against various types of viruses. The bactericidal effect is determined to strongly depend on the targeted virus types. It is evident that the disinfection becomes more ineffective with viruses less sensitive to the UV rays, i.e., smaller microorganism susceptibility. As can be observed, the effective sterilisation zone against *HIV* type is very small and formed very close to the lamp (see Figure 12c and Table 3); indeed, its radius is only of $r_e = 0.405$ m when the highest wattage, i.e., $P = 100$ W, is utilised, leading to a substandard disinfection in almost the whole room.

Furthermore, the larger the UV sensitivity, the further distance that the absolute disinfection ($b = 100\,\%$) against the virus takes place (see Figure 13). The bactericidal rate is extremely low at the most further location, i.e., at the surrounding walls; it is only 8.98 % against the *HIV* virus even when the disinfection is performed with a 100 W-lamp. It is good to point out that our simulation results are well in line with those obtained from an analytical approach in [24].

4. CONCLUSIONS

An investigation of the bactericidal effectiveness of a single UV lamp was conducted using a numerical approach. In this work, we targeted three different types of viruses: *Corona-SARS*, *Herpes* (type 2), and *HIV*. The lamp, whose wattage varied in the interval of $P = 30$–100 W, had a cylindrical shape and was

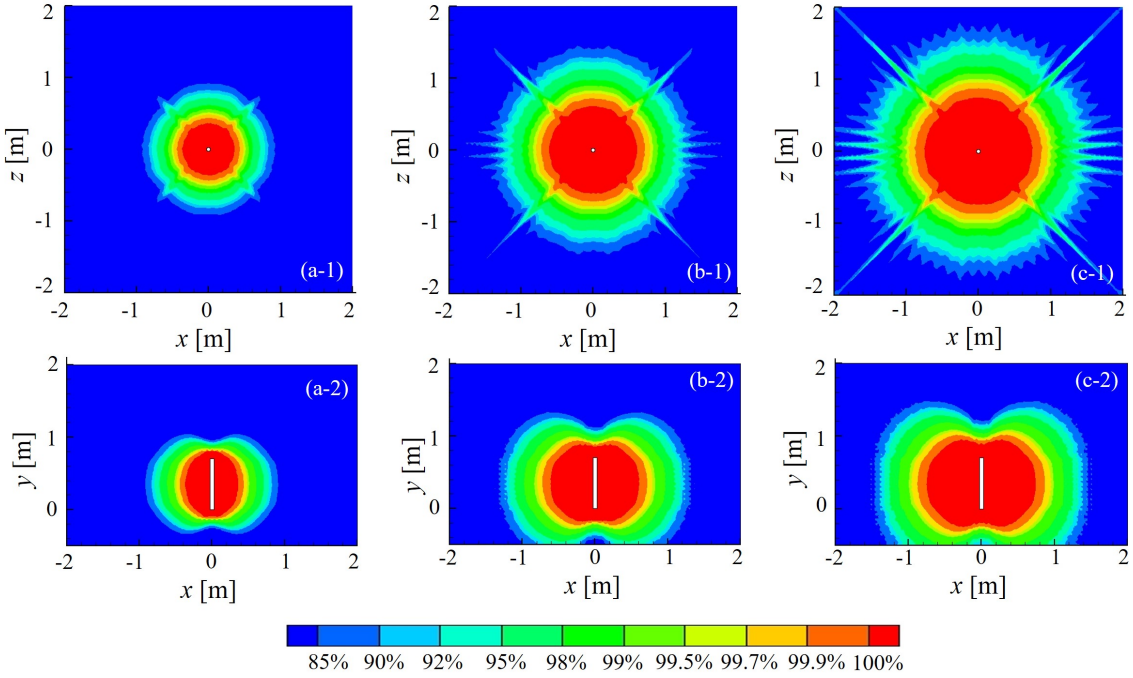

Figure 11. Bactericidal effect in (1) the xz-centerplane and (2) the xy-centerplane produced by a UV lamp of (a) 30 W, (b) 70 W, and (c) 100 W; the virus considered is of *Corona-SARS* type.

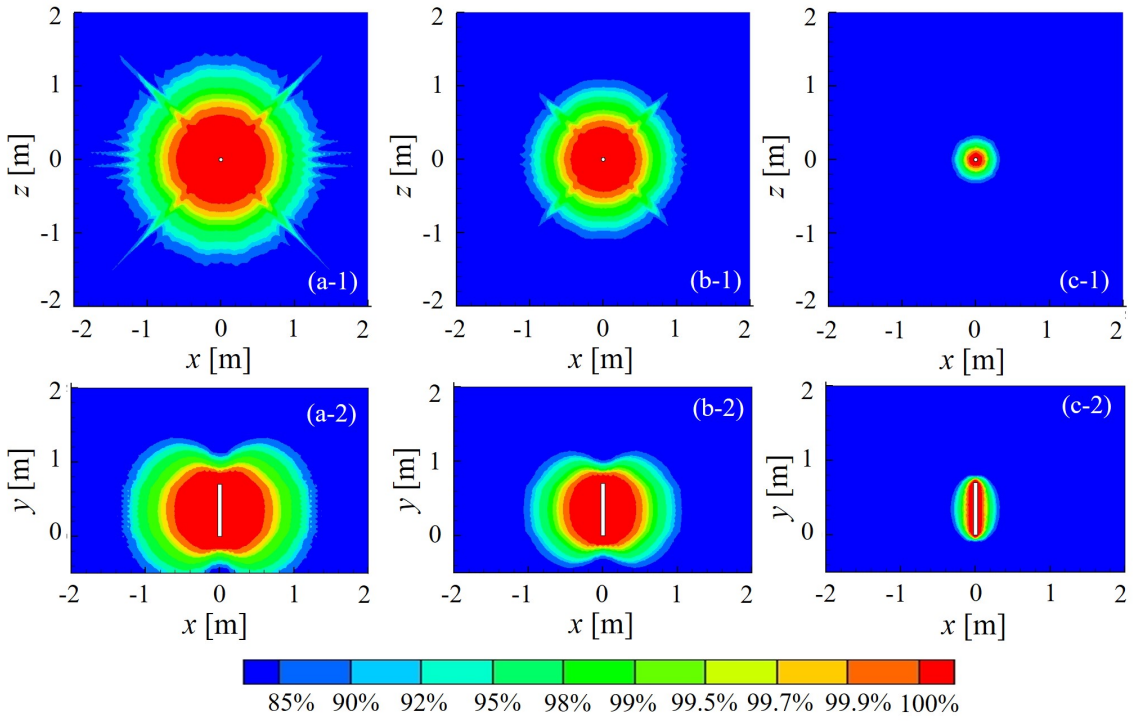

Figure 12. Bactericidal effect in (1) the xz-centerplane and (2) the xy-centerplane produced by a UV lamp of 70 W; the virus considered is of (a) *Corona-SARS*, (b) *Herpes*, and (c) *HIV* types.

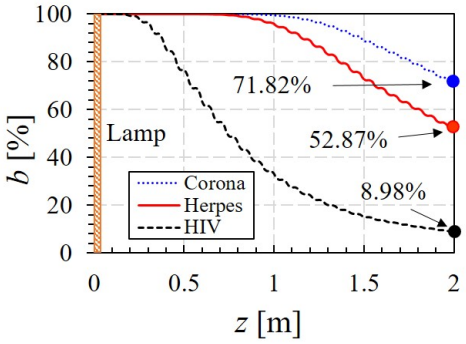

FIGURE 13. Bactericidal rate against various virus types as a function of the distance with the lamp power of 100 W.

placed in a vertical position. The UV irradiance was computed by the Finite Volume Method coupled with the Discrete Ordinates model; its modelling parameters were determined to be 3×3 and 15×15 for the pixelation and division sets, respectively.

For the radiation distribution, the UV intensity was observed to be reduced with an increase in distance to the lamp. Additionally, the lamp power was noted to have a strong effect on the UV distribution. Specifically, the higher the power, the larger the maximum intensity and significantly greater high-intensity zones around the lamp. With a 100 W-lamp, the zone within which $I \geq 50\,\mathrm{W/m^2}$ had a ∼2.6 times larger radius as compared to that created by a 30 W-one.

In addition, it was observed that the larger lamp wattage led to a greater bactericidal effect expressing the more efficient disinfection in the room. In detail, when compared to a 30 W-lamp, the radius of the effective sterilisation zone r_e was extended by ∼1.46 times and ∼1.76 times for the 70 W- and 100 W-ones, respectively. However, it is worth noting that the disinfection effectiveness was not as high in the whole room even when the highest wattage, i.e., 100 W, was used; this could result in the virus possibly surviving in the areas far away from the lamp. Moreover, the bactericidal performance could vary considerably according to the virus type. The lower the microorganism susceptibility, the smaller the bactericidal effects against the virus, and the smaller the effective sterilization zone. Furthermore, the bactericidal rate could be as low as approximately 8.98 %, at the surrounding walls for viruses less sensitive to UV rays such as the *HIV*.

Regarding future works, we plan to build experimental models and carry out a validation for our numerical approach. In addition, the effects of the airflow and temperature on the UV disinfection performance are also of interest.

List of symbols

P UV lamp wattage [W]
I UV intensity [$\mathrm{W/m^2}$]
I_0 Initial UV intensity [$\mathrm{W/m^2}$]
I_{max} Maximum UV intensity [$\mathrm{W/m^2}$]
r_e Effective sterilisation radius [m]
t Exposure duration [s]
b Bactericidal rate [%]
k Microorganism susceptibility [$\mathrm{m^2/J}$]

Acknowledgements

This research was funded by the People's Committee of Da Nang city, under a contract number 22/HĐ-SKHCN (2021).

References

[1] S. Ilyas, R. R. Srivastava, H. Kim. Disinfection technology and strategies for COVID-19 hospital and bio-medical waste management. *Science of the Total Environment* **749**:141652, 2020. https://doi.org/10.1016/j.scitotenv.2020.141652.

[2] Y. Ren, L. Li, Y.-m. Jia. New method to reduce COVID-19 transmission-the need for medical air disinfection is now. *Journal of Medical Systems* **44**(7):1–2, 2020. https://doi.org/10.1007/s10916-020-01585-8.

[3] S. M. Sharafi, K. Ebrahimpour, A. Nafez. Environmental disinfection against COVID-19 in different areas of health care facilities: a review. *Reviews on Environmental Health* **36**(2):193–198, 2020. https://doi.org/10.1515/reveh-2020-0075.

[4] J.-S. Chen. Enhancing air quality for embedded hospital germicidal lamps. *Sustainability* **13**(4):2389, 2021. https://doi.org/10.3390/su13042389.

[5] Z. Han, E. Pappas, A. Simmons, et al. Environmental cleaning and disinfection of hospital rooms: A nationwide survey. *American Journal of Infection Control* **49**(1):34–39, 2021. https://doi.org/10.1016/j.ajic.2020.08.008.

[6] M. Raeiszadeh, B. Adeli. A critical review on ultraviolet disinfection systems against COVID-19 outbreak: Applicability, validation, and safety considerations. *Acs Photonics* **7**(11):2941–2951, 2020. https://doi.org/10.1021/acsphotonics.0c01245.

[7] World Health Organisation, World Meteorological organisation, United Nations Environment Program, International Commission on Non-Ionising Radiation Protection. Global solar UV index : a practical guide, 2002.

[8] W. J. Kowalski, W. Bahnfleth, M. T. Hernandez. A genomic model for predicting the ultraviolet susceptibility of viruses. *IUVA news* **11**(2):15–28, 2009.

[9] B. Andersen, H. Bånrud, E. Bøe, et al. Comparison of UV C light and chemicals for disinfection of surfaces in hospital isolation units. *Infection Control & Hospital Epidemiology* **27**(7):729–734, 2006. https://doi.org/10.1086/503643.

[10] M. Bentancor, S. Vidal. Programmable and low-cost ultraviolet room disinfection device. *HardwareX* **4**:e00046, 2018. https://doi.org/10.1016/j.ohx.2018.e00046.

[11] P. Chanprakon, T. Sae-Oung, T. Treebupachatsakul, et al. An ultra-violet sterilization robot for disinfection. In *2019 5th International Conference on Engineering, Applied Sciences and Technology (ICEAST)*, pp. 1–4. IEEE, 2019. https://doi.org/10.1109/iceast.2019.8802528.

[12] M. Guettari, I. Gharbi, S. Hamza. UVC disinfection robot. *Environmental Science and Pollution Research* **28**:40394–40399, 2021. https://doi.org/10.1007/s11356-020-11184-2.

[13] A. Vyshnavi, A. Manasa, C. Hamsika, et al. UV disinfection robot with automatic switching on human detection. *EAI Endorsed Transactions on Internet of Things* **6**(23), 2020. https://doi.org/10.4108/eai.25-9-2020.166364.

[14] H. Pan, M. Orava. Performance evaluation of the UV disinfection reactors by CFD and fluence simulations using a concept of disinfection efficiency. *Journal of Water Supply: Research and Technology—AQUA* **56**(3):181–189, 2007. https://doi.org/10.2166/aqua.2007.101.

[15] C. Ho. Evaluation of reflection and refraction in simulations of ultraviolet disinfection using the discrete ordinates radiation model. *Water Science and Technology* **59**(12):2421–2428, 2009. https://doi.org/10.2166/wst.2009.260.

[16] H. Sobhani, H. Shokouhmand. Effects of number of low-pressure ultraviolet lamps on disinfection performance of a water reactor. *Journal of Water Process Engineering* **20**:97–105, 2017. https://doi.org/10.1016/j.jwpe.2017.08.021.

[17] A. Capetillo, C. J. Noakes, P. A. Sleigh. Computational fluid dynamics analysis to assess performance variability of in-duct UV-C systems. *Science and Technology for the Built Environment* **21**(1):45–53, 2015. https://doi.org/10.1080/10789669.2014.968512.

[18] F. Atci, Y. E. Cetin, M. Avci, O. Aydin. Evaluation of in-duct UV-C lamp array on air disinfection: a numerical analysis. *Science and Technology for the Built Environment* **27**(1):98–108, 2020. https://doi.org/10.1080/23744731.2020.1776549.

[19] Y. Yang, H. Zhang, A. C. Lai. Lagrangian modeling of inactivation of airborne microorganisms by in-duct ultraviolet lamps. *Building and Environment* **188**:107465, 2021. https://doi.org/10.1016/j.buildenv.2020.107465.

[20] A. G. Buchan, L. Yang, K. D. Atkinson. Predicting airborne coronavirus inactivation by far-UVC in populated rooms using a high-fidelity coupled radiation-CFD model. *Scientific reports* **10**(1):1–7, 2020. https://doi.org/10.1038/s41598-020-76597-y.

[21] N. Ropathy, H. L. Choo, C. H. Yeong, Y. H. Wong. UVC light simulation for room disinfection system. In *MATEC Web of Conferences*, vol. 335, p. 03012. EDP Sciences, 2021. https://doi.org/10.1051/matecconf/202133503012.

[22] Ansys, Inc. ANSYS FLUENT theory guide. *Canonsburg, Pa* **794**, 2011.

[23] E. Mitscherlich, E. H. Marth. *Microbial survival in the environment: bacteria and rickettsiae important in human and animal health*. Springer Science & Business Media, 2012. https://doi.org/10.1007/978-3-642-69974-0.

[24] N. D. M. Phan, N. Q. H. Tran, D. C. Tran, et al. An ultraviolet C light-emitting robot design for disinfection in the operating room. In *Recent Trends in Mechatronics Towards Industry 4.0*, pp. 185–196. Springer, 2022. https://doi.org/10.1007/978-981-33-4597-3_18.